Horne, Clare-Louise (2010) *Probing the dynamic scaling hypothesis in 1-D coarsening particle systems.* MSc(R) thesis.

http://theses.gla.ac.uk/1684/

Copyright and moral rights for this thesis are retained by the author

A copy can be downloaded for personal non-commercial research or study, without prior permission or charge

This thesis cannot be reproduced or quoted extensively from without first obtaining permission in writing from the Author

The content must not be changed in any way or sold commercially in any format or medium without the formal permission of the Author

When referring to this work, full bibliographic details including the author, title, awarding institution and date of the thesis must be given

Glasgow Theses Service
http://theses.gla.ac.uk/
theses@gla.ac.uk

Probing the Dynamic Scaling Hypothesis in 1-D Coarsening Particle Systems

Clare-Louise Horne

MSc (Research)
FIMS

November 8, 2009

1 Abstract

Hopefully this thesis will provide the reader with an idea of what coarsening is and when and where it may occur. The concise definition of coarsening that we employ is that characteristic length scales grow in time. The Dynamic Scaling Hypothesis which asserts that upon suitable scaling of space, features of late-time structures are indistinguishable is the main consideration in this thesis and we will investigate two 1-D coarsening dynamical systems, one for which The Dynamic Scaling Hypothesis holds and one for which it does not. This thesis studies, in particular, the coarsening-ballistic particle $\mathcal{CBP}$* model and the coarsening reverse-parabolic $\mathcal{CRP}$** model. We utilize an in-house code developed by Watson et al. to generate the morphometric data and we show that The Dynamic Scaling Hypothesis holds for the $\mathcal{CBP}$* model but does not hold for the $\mathcal{CRP}$** model. We also identify the existence of power law scaling and a scaling state in the $\mathcal{CBP}$* model which are not present in the $\mathcal{CRP}$** model. It is found in the $\mathcal{CRP}$** model however, that the distributions have a length scale dependence.

2 Introduction

2.1 General Background on Coarsening

A concise definition of coarsening is that characteristic length scales grow in time. Coarsening occurs when structures such as particles or drops meet and interact, and this may lead to the structures merging to form one larger structure or them being annihilated. Observed in many physical and social systems, computer simulations etc, coarsening is thus a decline in the number of structures while the distance between these structures increases. All of this is highlighted in the following diagram of grain coarsening, which arises in material science;

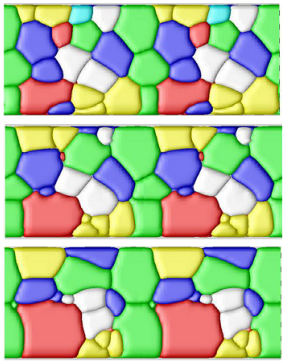

Figure 1: **Grain Coarsening**
At initial time, after 500 minutes and after 1000 minutes. [5]

Figure 1 highlights that as time increases the size of the grains is also getting larger but the number of grains is decreasing. Hence there is a growth of the characteristic length scale in time.

Figure 2 shows coarsening occurring in a 2-D foam and is an everyday life example indicative of foams [7, 8, 9, 10, 11, 12]. Foams are cellular materials that have gas bubbles dispersed randomly in a small amount of liquid. The liquid phase is connected but only covers a small volume fraction and the films forming the faces of the bubbles are called lamellae. Time begins when the gas is dispersed into the liquid. Due to gravity, the liquid in between bubbles drains away. After enough time has passed that the effect for the transient associated with the initial conditions is overcome, coarsening occurs as smaller bubbles become extinct, thus resulting in a growth of the characteristic length scale. This occurs due to the diffusion of gas from smaller bubbles to larger bubbles because of the difference in pressure. This results in the average bubble size increasing.

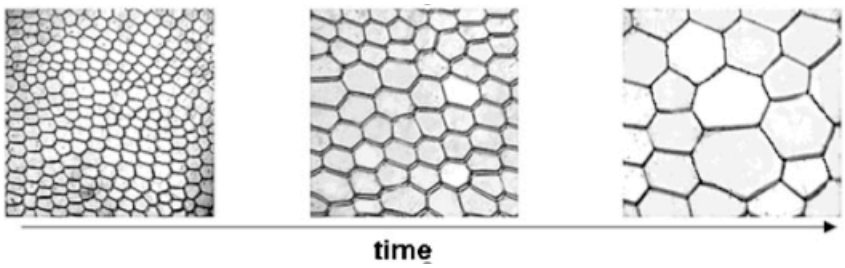

Figure 2: **Coarsening**
2-D foams at different times, illustrating coarsening. The arrow indicates the increase in time. The initial mean bubble diameter is D=1.5mm. [10]

Similarly to Figure 1, it can be seen from Figure 2 that as time elapses the average size of the foam bubbles increases, the number of bubbles has decreased, thus indicating that characteristic length scales grow in time.

Figure 3 is a simulation of coarsening of tin particles in a liquid lead-tin alloy. Again it is clear from Figure 3 that the number of tin particles is decreasing but the size of the particles is increasing as time passes and thus the characteristics required of coarsening are present.

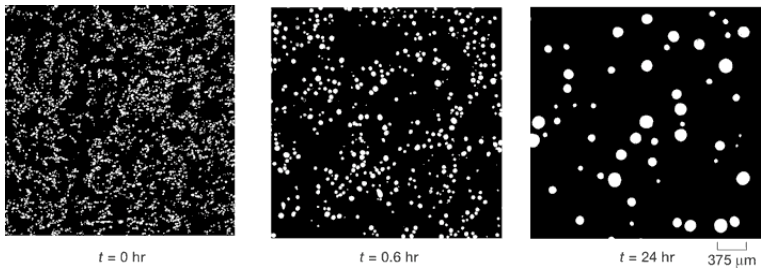

Figure 3: **Coarsening of Tin Particles**
At initial time, after 0.6 hours and after 24 hours. [6]

2.2 The Dynamic Scaling Hypothesis

The Dynamic Scaling Hypothesis (which is what we are concerned with in this thesis) asserts that upon suitable scaling of space, features of 'late-time' structures are indistinguishable. The interpretation of 'late-time' is that sufficient time has lapsed to allow the effects of initial conditions to have faded. If an insufficient amount of time has passed there will be a transient present associated with the initial conditions. Hence there has to be a enough structures, such as particles, droplets or bubbles to interact with each other so that this transient is overcome. This will be explored in the latter pages of this thesis. One signature which may generally arise from The Dynamic Scaling Hypothesis is a power law scaling which connects length scale and time.

There have been many studies on the topic of coarsening and coarsening occurs regularly in everyday life, such as in clouds, shaving foams etc [13, 14]. To illustrate the issues central to this thesis, we will examine in detail the example of breath figures [1, 2, 3, 4]. Breath figures are the patterns formed by water droplets when they enlarge and coalesce, e.g. dew on grass or condensation on windows or spectacles. Breath figures display three stages through which the patterns emerge. Firstly, the droplets grow individually (the diameter of a droplet is growing as a power law in time) and the distance between the droplets is large in comparison to their size. In this first stage, where no coalescence occurs, there is a transient present associated with the initial conditions. In the second phase, the distance between the droplets is comparable to their size, and so they ultimately coalesce. Mass is conserved when two such droplets coalesce. This phase where coarsening occurs is highlighted in Figure 4.

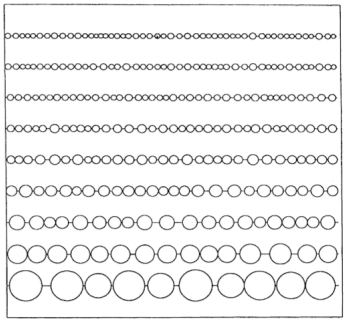

Figure 4: **Coarsening**
Simulation of the one-dimensional D=3 droplet model: patterns obtained starting with 1000 droplets, for final states of 50, ..., 10 droplets left. [2]

An extremely interesting feature is that the breath figures exhibit 'self-similarity'.

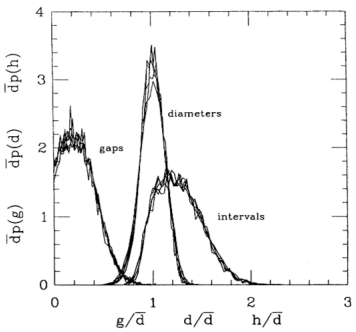

Figure 5: **Self-similarity**
Distributions of lengths of intervals, diameters, and gaps, in the one-dimensional D=3 droplet model, at five different times in the constant coverage regime corresponding to 10000, 9000, 8000, 7000, 6000 droplets left.[2]

'Self-similarity' means that upon suitable scaling of space, features of late-time structures are indistinguishable. In Figure 5, intervals are the distances between centers of neighbouring droplets, diameters are straightforward and gaps are the distances between droplets which Figure 6 highlights. Figure 5 shows a family of realisations which are scaled by the average diameter at each time but averaging is not carried out and error bars are not plotted. The data we acquire in this thesis will be averaged and error bars will be present resulting in higher levels of confidence in our results.

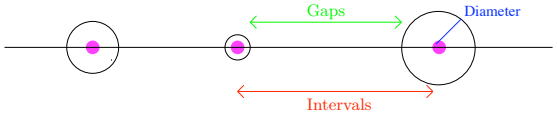

Figure 6: **Intervals, Diameters, Gaps**

The thesis studies two classes of 1-D coarsening dynamical systems. Namely, the coarsening-ballistic particle $\mathcal{CBP}$* [14] and coarsening reverse-parabolic $\mathcal{CRP}$** [15] models. We will be utilizing an in-house code developed by Watson et al. to generate the morphometric data and we will show that The Dynamic Scaling Hypothesis holds for the $\mathcal{CBP}$* model. In particular, we will identify power law scaling and associated scaling functions. Since we find that a scaling state appears to exist, laws governing features of the scaling state will be identified. Furthermore, we will also output late-time distributions that are self-similar and we have error estimates present which highlight that our information is highly accurate. However, we will find strong evidence that the $\mathcal{CRP}$* model does not satisfy The Dynamic Scaling Hypothesis. In particular, we will highlight that there is no power law scaling and we will present late-time distributions which are not self-similar. It will be shown though, that the distributions of the $\mathcal{CRP}$* model have a length scale dependence.

3 *The $\mathcal{CBP}$ model

The coarsening-ballistic particle ($\mathcal{CBP}$) model examines the fate of N_k particles of total mass M on a periodic domain of length L for which each particle of mass m travels with velocity $\mathscr{V}$ according to

$$\mathscr{V} = \mathscr{F}(m)$$

where $\mathcal{F}$ is a prescribed function, and particles which meet follow the coarsening law

$$m_{\text{left}} \bullet\!\!-\!\!\bullet\, m_{\text{right}} \longrightarrow \bullet\, m_{\text{new}} = m_{\text{left}} + m_{\text{right}}.$$

For a prescribed total mass M and domain length L, we will aim to obtain the scaling laws and associated scaling functions (the pdf's) for the range of velocity laws;

$$\mathcal{F}(m) = \frac{1}{m^p},$$

for velocity exponents $p > 0$. Also, laws governing features of the scaling state will be identified.

The equivalent convection-corrected velocity law is

$$\mathcal{V}^{(k)}(m) = \mathcal{F}(m) - \frac{1}{N_k}\sum_{j=1}^{N_k} \mathcal{F}(m), \tag{1}$$

which factors out a net-drift which will be of use in plotting the coarsening pathway.

3.1 Overview

In the next section I am going to consider general information about the $\mathcal{CBP}$ model; reducing it to the canonical problem and highlighting how it is suitable to analyse the model with a large but finite number of particles. Following on from this, I will determine if and when a scaling state occurs and provide further information on the scaling state. Also, I will examine the probability density functions (pdf's) produced and identify emergent features that they have. The pdf's will all be plotted with errors. The errors will be calculated in two ways to show consistency of the numerical results - the histogram method and the Kernel Density method. Both ways will be examined but I will try to fit functions to the Kernel Density method.

3.2 The Model

Remark 1 *We scale the problems, where possible to characteristic (representative) problems; e.g., for the special case* $\mathcal{F}(m) = \frac{1}{m^p}$*, a suitable re-scaling of length, masses and time matches the general problem (i.e., with M and L) maps to the characteristic problem with* $L = 1$ *and* $M = 1$*.*

$$\frac{dx_i}{dt} = \frac{1}{m_i{}^p} \tag{2}$$

Now, we intend to scale x_i, m_i and t as follows:

$$x_i = LX_i \tag{3}$$

$$m_i = MM_i \tag{4}$$

$$t = \hat{t}T \tag{5}$$

It is clear that (3) enforces the particles to live on a domain $[0, 1]$, and (4) ensures that the total particle mass is 1. It is quite obvious that these scalings should go a long way to simplifying our problem. Next, if we substitute these scaled parameters into (2), we see that

$$\frac{L}{\hat{t}}\frac{dX_i}{dT} = \frac{1}{M^p}\frac{1}{M_i^p}.$$

We are free to choose any value for $\hat{t}$, so it seems sensible to attach the value $\hat{t} = M^p L$. Then

$$\frac{dX_i}{dT} = \frac{1}{M_i^p}. \tag{6}$$

Now (6) represents our canonical problem. So in summary,

Canonical Problem:

$$\frac{dX_i}{dT} = \frac{1}{M_i^p} \qquad X_i(T) \in [0, 1] \qquad \sum_{i=1}^{N} M_i = 1$$

Now, using this canonical problem, we can now solve any problem of interest with any specifications of M and L.

Suppose we have an infinite number of particles on the real line. Then the set of all particles can be represented by $\{ x_i \, ; i \in \mathcal{I} \}$ where $\mathcal{I} \subset \mathbb{Z}$ and $\mathcal{I}$ is the index set, and x_i is the location of the i-th particle. The location of each particle is dependent on time and so will be written as $x_i(t)$. This is shown in Figure 7. So at time $t = 0$ the i-th particle would have location $x_i(0) = \bar{x}_i$, which is specified. The average distance between particles is given by $<d>(t)$.

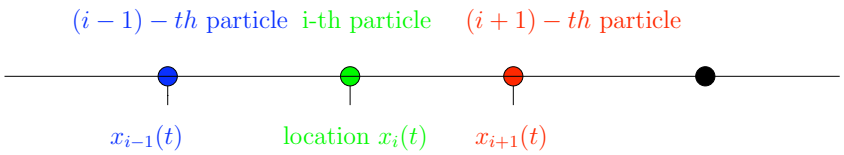

Figure 7: **Particles on a Line**
$x_{i-1}(t) < x_i(t) < x_{i+1}(t)$.

Remark 2 *In practice, we actually carry out the calculations with a finite number of particles on a periodic domain of length L. The number of particles at time t is denoted by N(t), shown in Figure 8.*

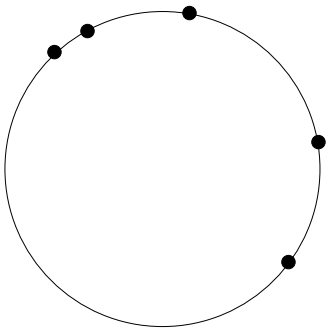

Figure 8: **Particles on a periodic domain of length** L

This makes sense and is accurate as long as L is much greater than $<d>(t)$ *ie* $<d>(t) << L$. *This condition* $<d>(t) << L$ *is known as the Separation of Scale condition and "emulates" the infinite problem. However if* $<d>(t) \to L$, *finite scale effects arise and we no longer have an infinite number of particles. Obviously, represented in this way* $<d>(t) = \frac{L}{N(t)}$ *and thus substituting this into the separation of scale condition gives* $\frac{L}{N(t)} << L$ *ie* $1 << N(t)$ *which also models "infinitely many" particles. So therefore as long as* $1 << N(t)$ *we are fine to carry out the calculations with a finite number of particles. Our numerical results identify how large* $N(t)$ *has to be to get robust statistics.*

In the case of the $\mathcal{CBP}$ model, particles interact only through coalescence. This places $\mathcal{CBP}$ within the general framework of 1-D coarsening particle systems. Namely, systems where when particles meet they either generate new particles or annihilate particles. The coarsening regime arises when the number of particles that emerge after interaction is always less than the number before.

This can be written as

$$n \xrightarrow{\oplus} outcome,$$

where n is the number of particles and $\oplus$ is a coarsening rule. Thus

$$n_{meet} \xrightarrow{\oplus} n_{out}, \qquad n_{out} < n_{meet}.$$

A representative trajectory of a realisation of $\mathcal{CBP}$ is shown in Figure 9.

In $\mathcal{CBP}$, the generic coarsening event is two particles meet and merge into one particle at many different times and locations, until one remains. The masses and locations of the particles are randomly chosen and this is carried out by another program which provides us with random numbers subject to some distribution. We selected a uniform distribution so the program picks a number between 0 and 1 and sends it to our program. Once our program receives this number it subtracts 0.5 from it. Thus we end up with a random number between -0.5 and 0.5 which is uniformly distributed - the whole range is equally likely to come up. It then takes this number and scales it to the size of the problem, the particles locations are distributed evenly and then 'bumped' by some random factor which is quite small in size. Similarly, the masses are done by getting another random number from the same program for each particle and setting its mass to this. Hence they all have mass between 0 and 1 with any number coming out with equal probability. Then, the program scales the masses so that the total mass is 1.

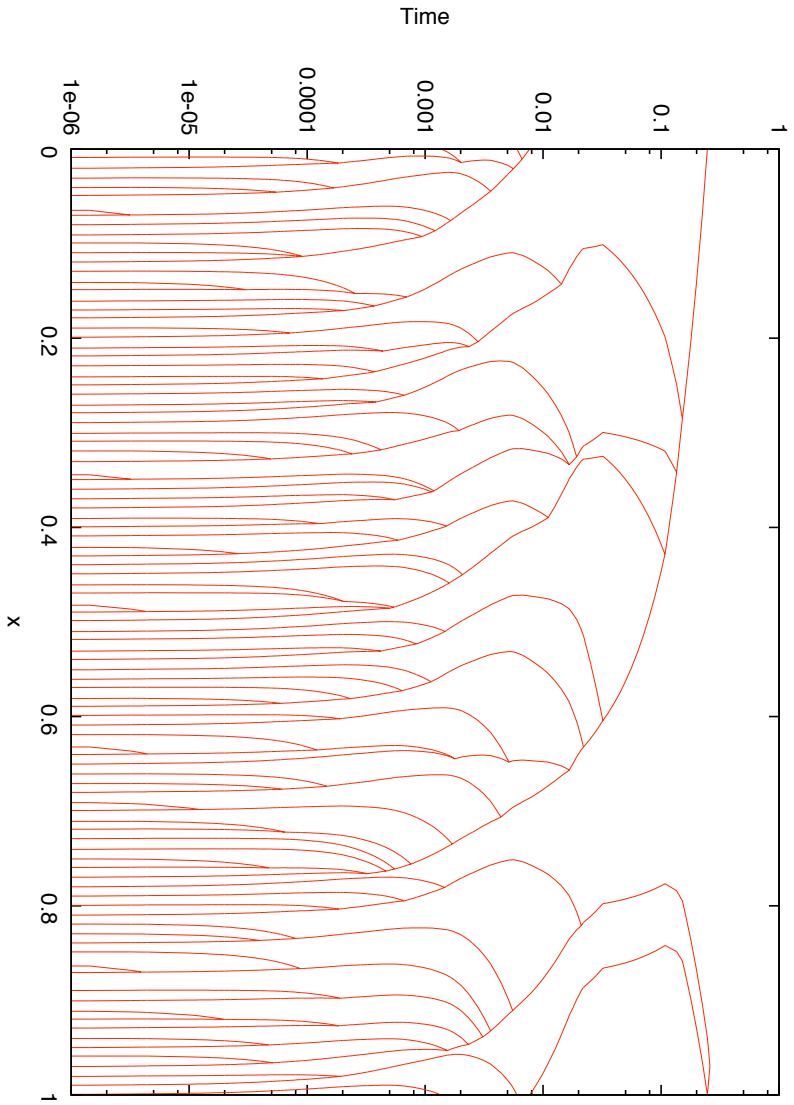

Figure 9: **Representative Coarsening Pathway for $\mathcal{CBP}$**
Starting from 100 particles with randomly selected masses and locations. Note here that we are using the convection-corrected velocity law (1).

3.3 The Scaling Hypothesis

We now probe the scaling properties of the coarsening dynamical system associated with $v_i = \frac{1}{m_i{}^p}$. Since the average length and mass scale with the number of particles, they must scale the same way. Consider the following scalings of t, l and m;

$$t \longrightarrow \lambda^q t \tag{7}$$

$$l \longrightarrow \lambda l \tag{8}$$

$$m \longrightarrow \lambda m \tag{9}$$

where q is a given constant. It follows from our assumed velocity law that

$$\frac{\lambda^{p+1}}{\lambda^q} v_i = \frac{1}{m_i{}^p},$$

and so the choice $q = p + 1$ leaves $v_i = \frac{1}{m_i{}^p}$ invariant. So, if the system displays dynamic scaling, the only temporal scaling laws for the average mass and average length consistent with the above scale invariance are

$$<m> \sim t^{\frac{1}{p+1}} \qquad \text{and} \qquad <l> \sim t^{\frac{1}{p+1}}$$

We say that the (temporal) scaling exponent n for the p'th power velocity law, $v_i = \frac{1}{m_i{}^p}$, is $n = \frac{1}{p+1}$. We now probe wether the predicted scaling exponent $n = \frac{1}{p+1}$ indeed arises through a numerical study.

3.4 Probing the Scaling Hypothesis for the case $v_i = \frac{1}{m_i}$

As the number of particles after coarsening decreases, then $<d>(t)$ increases as $<d>(t) = \frac{1}{No. of particles}$. We want to compute what $<d>(t)$ is approximately equal to

and how quickly it increases. We can see from the following graph that $<d>(t)$ is increasing as the No. of particles is decreasing. On a log/log scale

$$<l> \sim t^{\frac{1}{p+1}}$$

presents itself as a linear relation

$$ln \ <l> \sim \frac{1}{p+1} ln \ t$$

so we may identify the scaling exponent by plotting log $<l>$ versus log t (a so called log/log plot) and reading off the slope of the straight line that emerges. It turns out that no matter what initial conditions etc that we have, we get the following sort of graph seen in Figure 10;

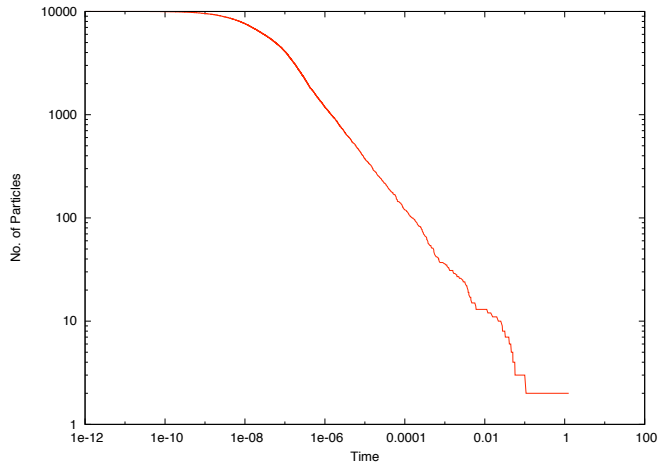

Figure 10: **Number of Particles, N(t) against Time**
Log/log plot. The location and masses of the initial particles are randomly chosen and $N(0) = 10000$. In this case the velocity is $v_i = \frac{1}{m_i}$.

3.5 Description of Behaviour

As can be seen from Figure 10, if the No. of particles is plotted against Time, there is a part of the graph where it straightens out and this suggests a power law. The graph in Figure 10 has 10000 particles at the start but the graph has the same shape regardless of the No. of particles at the start. This highlights that there is universality as all the graphs behave in the same way. Just to clarify this, the following graph, in Figure 11, shows the behaviour for 10000, 25000 and 50000 particles at the start;

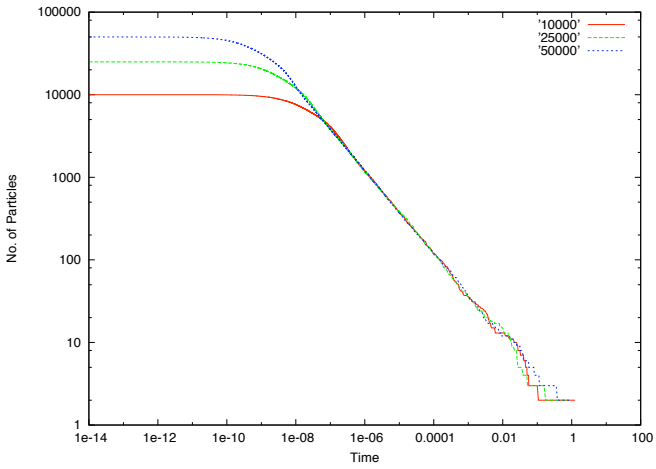

Figure 11: **Number of Particles, N(t) against Time**
Log/log plot. The key on the graph shows that the red line is for $N(0) = 10000$, green is for $N(0) = 25000$ and blue is for $N(0) = 50000$. Again, the initial locations and masses are chosen randomly and the velocity is $v_i = \frac{1}{m_i}$.

Figure 11 therefore answers the question of how large $N(t)$ must be for the statistics to be robust. It is obvious that $N(t) = 10000$ is sufficient.

From Figure 12 it is seen that the slope of the power law for the velocity law $v_i = \frac{1}{m_i}$ is $-\frac{1}{2}$.

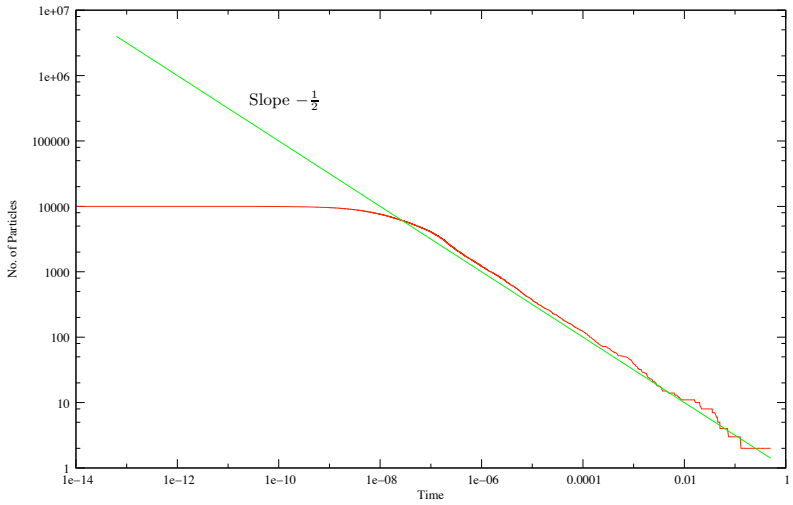

Figure 12: **Slope of Power Law**
Log/log plot. The location and masses of the initial particles are randomly chosen and $N(0) = 10000$. The graph of No. of Particles against Time is for the velocity $v_i = \frac{1}{m_i}$ and the other line is of slope $-\frac{1}{2}$.

Thus power law behaviour is displayed and in this case, $N(t) = t^p$ where $p = -\frac{1}{2}$.

3.6 Probing the Scaling Hypothesis for the case $v_i = \frac{1}{m_i^p}$

We now assign each of the particles on the real line a mass, m_i. The velocity of the particle, v_i, is determined by it's mass and thus $v_i = f(m_i)$, where f is a given function. Eg. $f(m_i) = \frac{1}{m_i}$, which implies that heavier particles move slower and lighter particles move faster. Again we consider the particles to be on a curve and if we have two particles m_i and m_{i+1} on the circle that meet, they follow the coarsening law

$$m_i \bullet\!\!-\!\!\bullet\, m_{i+1} \longrightarrow \bullet\, m_{\text{new}} = m_i + m_{i+1}.$$

All of the data we have recorded before is taking the velocity, $v_i = \frac{1}{m_i}$. The parameter that we can vary, however, is the velocity exponent and if we take $v_i = \frac{1}{(m_i)^2}$, then the graph of No. of Particles against Time for 10000 particles at the start is shown in Figure 13, along with the associated power law.

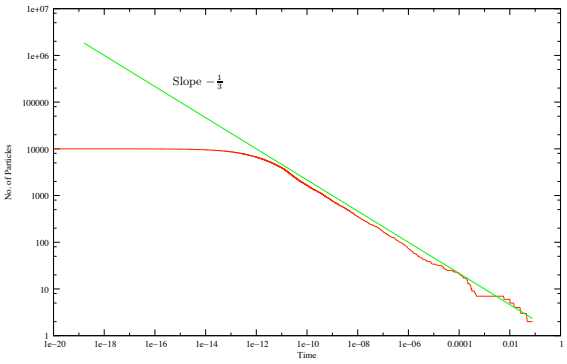

Figure 13: **Slope of Power Law**
The location and masses of the initial particles are randomly chosen and $N(0) = 10000$. The log/log plot of No. of Particles against Time is for the velocity $v_i = \frac{1}{(m_i)^2}$ and the other line is of slope $-\frac{1}{3}$.

Thus from the log/log plot appearing in Figure 13 it is seen that the slope of the power law for the velocity law $v_i = \frac{1}{(m_i)^2}$ is $-\frac{1}{3}$. So in this case $N(t) = t^p$ where $p = -\frac{1}{3}$.

Furthermore, taking $v_i = \frac{1}{(m_i)^3}$, then the graph of No. of particles against Time for 10000 particles at the start is shown in Figure 14, along with the associated power law.

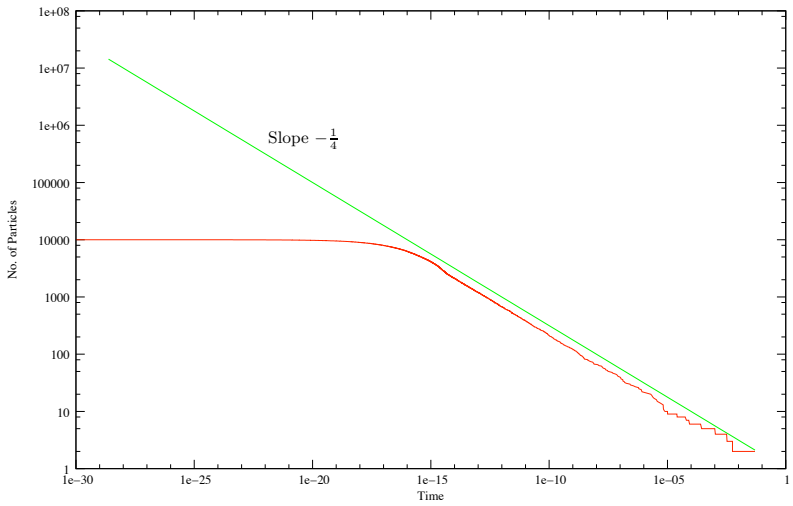

Figure 14: **Slope of Power Law**
The location and masses of the initial particles are randomly chosen and $N(0) = 10000$. The log/log plot of No. of Particles against Time is for the velocity $v_i = \frac{1}{(m_i)^2}$ and the other line is of slope $-\frac{1}{4}$.

Hence from Figure 14 it is seen that the slope of the power law for the velocity law $v_i = \frac{1}{(m_i)^2}$ is $-\frac{1}{4}$. This means that in this case $N(t) = t^p$ where $p = -\frac{1}{4}$.

Lastly, from Figure 15, obviously using the same pattern as has been shown previously, the slope of the power law for the velocity law $v_i = \frac{1}{(m_i)^9}$ is $-\frac{1}{10}$. So here $N(t) = t^p$ where $p = -\frac{1}{10}$.

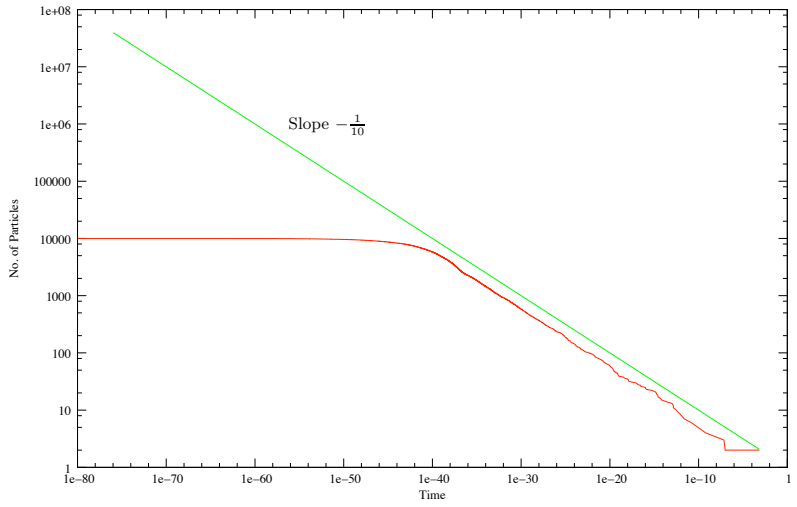

Figure 15: **Slope of Power Law**
The location and masses of the initial particles are randomly chosen and $N(0) = 10000$. The log/log plot of No. of Particles against Time is for the velocity $v_i = \frac{1}{(m_i)^9}$ and the other line is of slope $-\frac{1}{10}$.

Since we do observe $<l> \sim t^{\frac{1}{p+1}}$, this suggests the system is displaying dynamic scaling behaviour and the conclusion we can draw from this is that power law behaviour persists but the exponents change. So, if we just change the notation slightly by incorporating the minus sign into $N(t) = t^p$ we now have $N(t) = t^{-p}$. From now on we shall call n the Scaling Exponent. Also, we have $v_i = \frac{1}{m_i{}^p}$, where we shall call p the Velocity Exponent. Figure 16 shows the relationship between n and p and it is obvious that $n = \frac{1}{p+1}$.

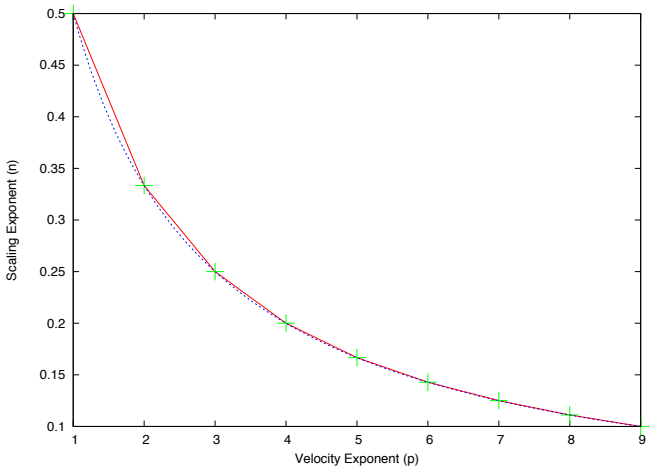

Figure 16: **Scaling Exponent (n) against Velocity Exponent (p)**
The blue line is $n = \frac{1}{p+1}$ and the red line is generated from the above findings.

In general, it is clear from all of the above graphs that as the power we raise m_i to increases, then the particles enter the power law state quicker and this is because the velocity is greatly increased each time we raise the power. To get this result though, there has to be enough particles to interact through collisions.

3.7 Deeper Probing of the Scaling Hypothesis and Associated Scaling State

We now look at deeper probes of the scaling hypothesis. Namely we look at a suitably scaled family of distributions, outputted at various points in the believed scaling state to see if they are invariant. A signature of the scaling state is the part of the graph where there is an observed scaling law (see Figure 17). This is where we sample statistics and from now on we shall call the No. of Particles at the start of the believed scaling state N_s and at the end of the believed scaling state N_f.

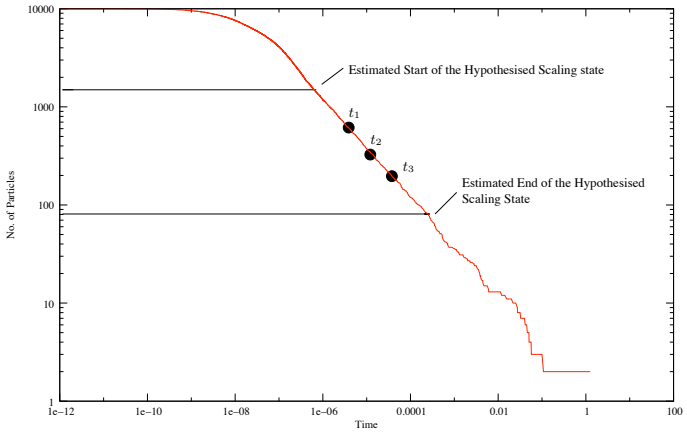

Figure 17: **Schematic of Sample Times for examining the Scaling Functions** Here we have $N(0) = 10000$, $v_i = \frac{1}{m_i}$, and t_1, t_2, t_3 are all in the conjectured scaling state. N_s and N_f are estimated by the points where the horizontal lines touch the vertical axis.

In Figure 18, the following distributions are outputted at t_1, t_2, t_3;

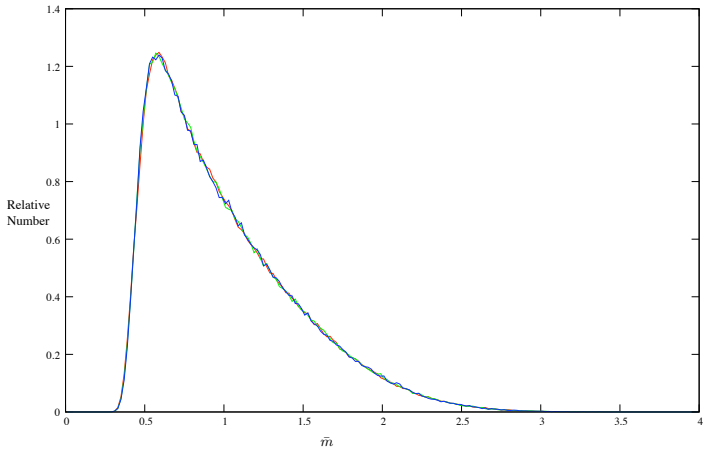

Figure 18: **Family of Mass Distributions**
t_1, t_2, t_3 are all in the conjectured scaling state. $N(0) = 10000$ and $v_i = \frac{1}{m_i}$. The red line is outputted at t_1 when 820 particles remain, the green at t_2 when 640 particles remain and the blue at t_3 when 460 particles remain.

Hence it is obvious from the Figure 18 that, in the case $v_i = \frac{1}{m_i}$, the scaled mass distributions are consistent and hence dynamic scaling occurs.

3.8 Generating Data Relevant to the Scaling State

Before proceeding to large scale acquisition of data we examine the signatures of dynamic scaling which can be utilised for efficient harvesting of scaling states. We will argue here that fractional loss of particles is a good scheme for identifying the scaling state. To estimate where the scaling state begins and ends it is required that a few graphs are analysed. It is straightforward from Figure 17 to estimate where the scaling state occurs and then a straight

line is drawn from these points over onto the vertical axis. This then gives us N_s and N_f and if N_s and N_f are divided by $N(0)$ - the initial No. of particles then the resulting numbers, $\frac{N_s}{N(0)}$ and $\frac{N_f}{N(0)}$, are a fraction of $N(0)$. Hence, at the start of the scaling state there is approximately 1500 particles left, giving $\frac{N_s}{N(0)} = \frac{1500}{10000} = 0.15$ and at the end of the scaling state there is 80 particles left, giving $\frac{N_f}{N(0)} = \frac{80}{10000} = 0.008$. The following table shows these results for varying numbers of particles at the start, $N(0)$ and corresponding $\frac{N_s}{N(0)}$ and $\frac{N_f}{N(0)}$.

$N(0)$	$\frac{N_s}{N(0)}$	$\frac{N_f}{N(0)}$
10000	0.15	0.008
20000	0.175	0.00375
25000	0.17	0.0112
50000	0.11	0.007
150000	0.186666666	0.003633333

Figure 19: **Shows $N(0)$ and corresponding $\frac{N_s}{N(0)}$ and $\frac{N_f}{N(0)}$ for $v_i = \frac{1}{m_i}$.**

We now turn to examining the fractional loss criteria for the other velocity laws $v_i = \frac{1}{m_i{}^p}$. However, it is shown from Figure 20 that as we increase the Velocity Exponent (p), the fractional loss required to enter the scaling state is approximately the same.

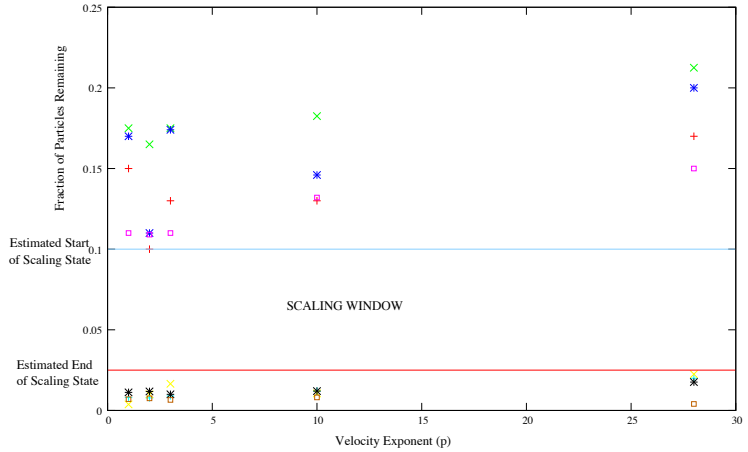

Figure 20: **Estimated Start and End of Scaling State**
The following is a key showing that the different point styles highlight the No. of Particles at the start, $N(0)$; + denotes $N(0) = 10000$, x denotes $N(0) = 20000$, * denotes $N(0) = 25000$ and the square point denotes $N(0) = 50000$. The red line marks the fractional loss of particles, 0.025, at which we exit the scaling state, while the light blue line marks the fractional loss of particles, 0.1, at which we enter the scaling state.

Hence, we could estimate that when there is between $\frac{1}{10}$ and $\frac{1}{40}$ of the No. of particles that there was at the start, then we are in the scaling state. To enable the program to run with 10000 - 50000 particles at the start, we cannot raise the power of m_i to anything higher than 28. Above 28, the program is unable to cope as the numbers it has to deal with are getting too large.

3.9 The Scale Invariant Distributions for Mass and Length

We now turn to the large-scale acquisition of data on scaling states utilising the fractional loss criteria for sampling. Here if we let $N_i(t)$ be the No. of Particles, $<m>(t)$ be the average mass and $m_i(t)$ be the current mass, then it is obvious that

$$<m>(t) = \frac{1}{N_i(t)}$$

and we can introduce

$$\bar{m_i} = \frac{m_i(t)}{<m>(t)}$$

which is the new mass relevant to the current average. The program then has to add each mass ($\bar{m_i}$) into the corresponding bin and then the data can be plotted to get a histogram. Figure 21 shows the distribution of mass relevant to the current average and is a generic example for m^1. The support is the distance between the two points on the graph. The point at the end of the Vacuum Interval, denoted V_1, is that point after which the recorded mass distribution is non-zero; we shall sometimes call this the **Start Value**. Similarly, the **End Value** is that point after which the recorded mass distribution is zero. In general, we will denote the start value associated with the *pth* power velocity law, $v_i = \frac{1}{m_i^p}$, V_p.

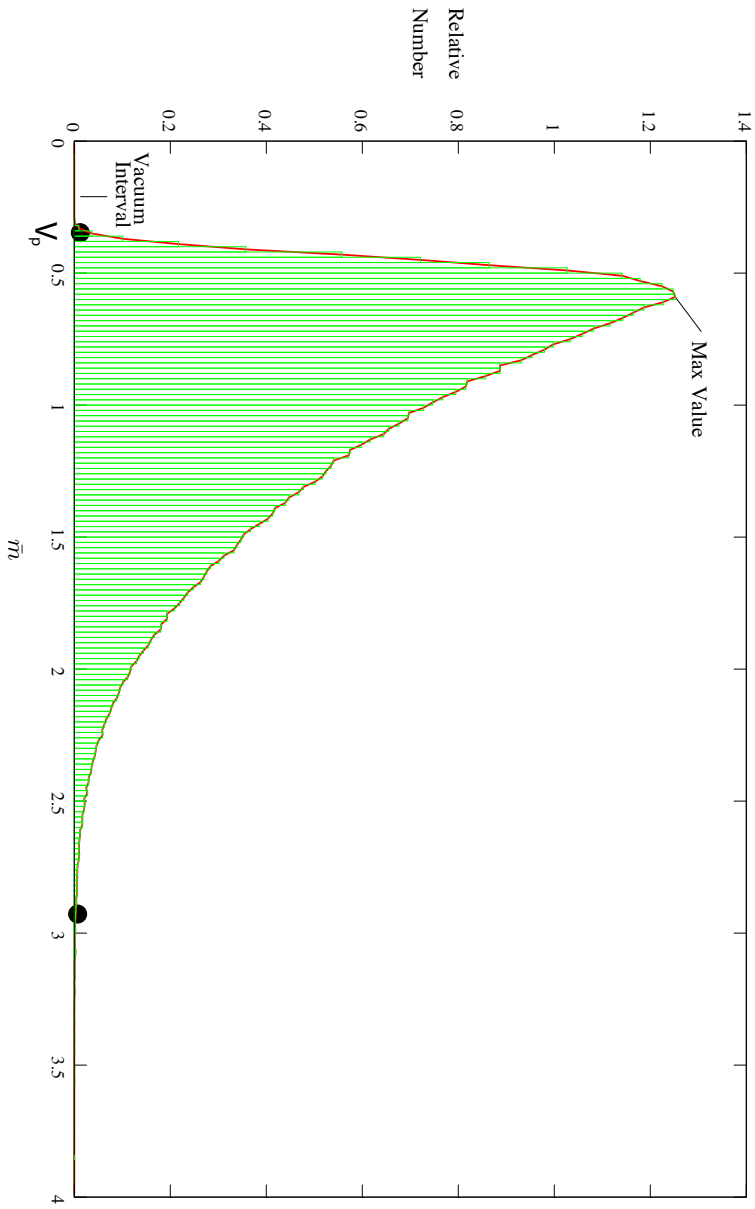

Figure 21: **Distribution of Mass Relevant to Current Average**
Highlights the distribution of mass relevant to the current average for the velocity $v_i = \frac{1}{m_i}$. The start and end values of the support of the distribution are clearly marked by the black dots, and the start value is denoted V_p where $p = 1$ in this case.

Furthermore, the following graph (Figure 22) is a generic example of the distribution of lengths relevant to the current average, for m^1;

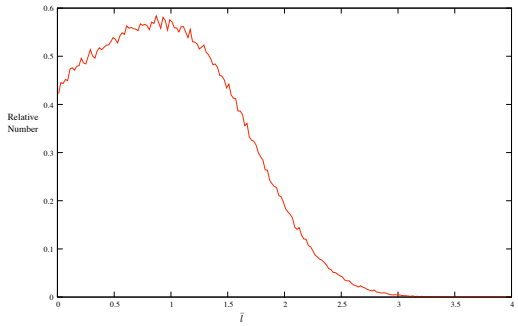

Figure 22: **Distribution of Length Relevant to Current Average**
Highlights the distribution of length relevant to the current average for the velocity $v_i = \frac{1}{m_i}$ in the same way as Figure 21 does for mass.

However we can vary the Velocity Exponent (p) and Figure 23 shows how the expected mass distributions vary as we do this;

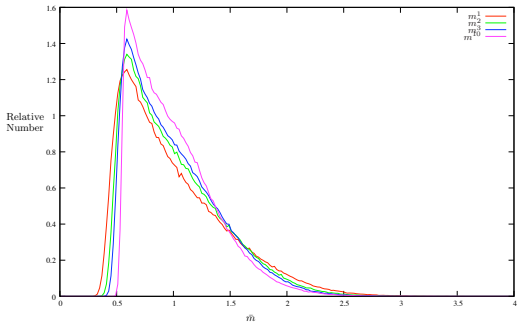

Figure 23: **Expected Mass Distributions**
Expected mass distributions for various velocity exponents. The key on the graph highlights that the velocities are $v_i = \frac{1}{m_i}, v_i = \frac{1}{(m_i)^2}, v_i = \frac{1}{(m_i)^3}, v_i = \frac{1}{(m_i)^{10}}$.

Obviously from Figure 23 it is clear that the vacuum state (where there is absolutely no mass recorded) extends as we increase the Velocity Exponent (p). Similarly, although we focus on the mass distributions, the length distributions can be analysed in the same way (ran the same number of times as the mass distributions and smoothed in the same way). Figure 24 shows how the expected length distributions vary as we alter the Velocity Exponent (p).

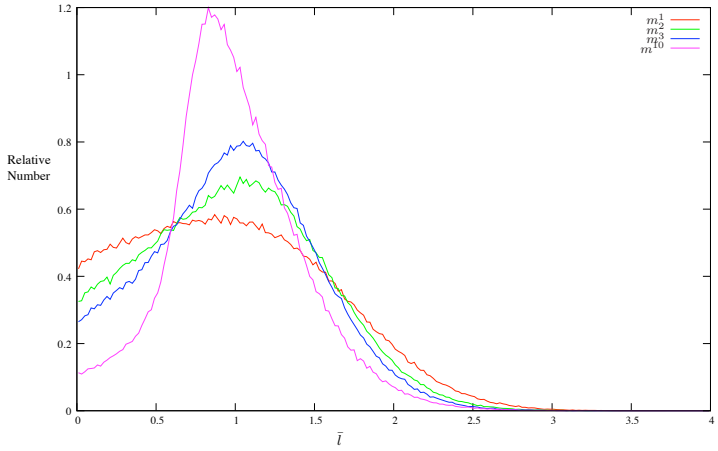

Figure 24: **Expected Length Distributions**
Expected length distributions for various velocity exponents. The key on the graph highlights that the velocities are $v_i = \frac{1}{m_i}, v_i = \frac{1}{(m_i)^2}, v_i = \frac{1}{(m_i)^3}, v_i = \frac{1}{(m_i)^{10}}$.

3.10 Error Analysis - Quantifying the Errors in our Distributions

Moreover, the program has been set up to calculate the standard error using the formula;

$$SE_{\mathcal{H}} := \sqrt{\frac{Var_N X}{N}} \quad \text{where} \quad Var_N X = \frac{1}{N}\sum_{i=1}^{N}(X_i - \bar{X_N})^2.$$

If we let $R(\bar{m})$ be the relative number of particles of scaled mass $\bar{m}$ then we have an upper error function, $R^+(\bar{m}) = R(\bar{m}) + SE_{\mathcal{H}}(\bar{m})$ and a corresponding lower error function, $R^-(\bar{m}) = R(\bar{m}) - SE_{\mathcal{H}}(\bar{m})$. These are the values which are used to calculate the error envelope. Hence Figure's 25 and 26 show the expected distributions for different Velocity Exponents (p) with error envelope included;

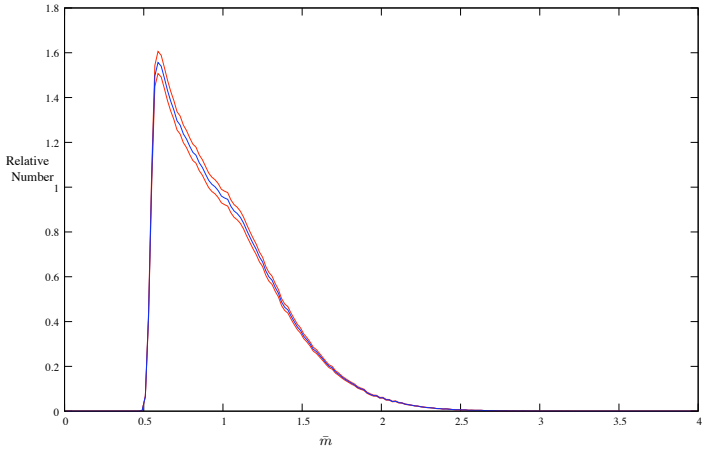

Figure 25: **Expected Mass Distribution with Errors**
This is for the velocity $v_i = \frac{1}{(m_i)^{10}}$. The blue curve is the expected distribution and the red curve above the expected distribution is $R^+(\bar{m})$ and the one below the expected distribution is $R^-(\bar{m})$.

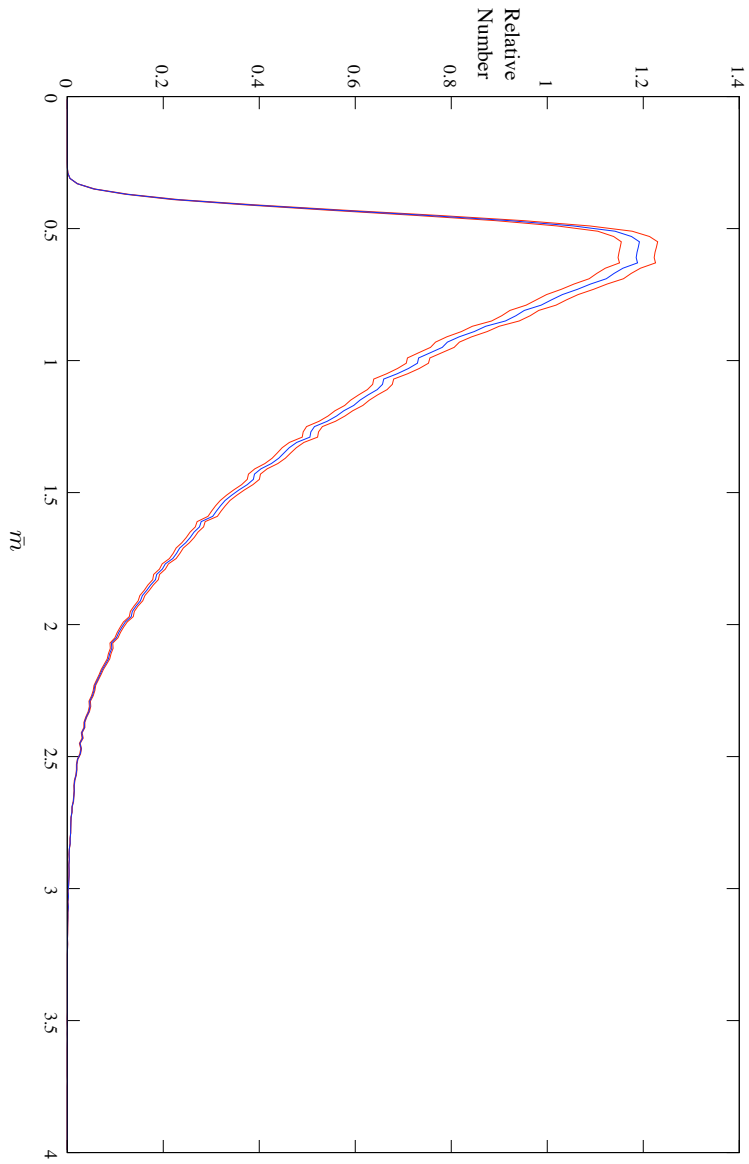

Figure 26: **Expected Mass Distribution with Errors**
This is for the velocity $v_i = \frac{1}{m_i}$. The blue curve is the expected distribution and the red curve above the expected distribution is $R^+(\bar{m})$ and the one below the expected distribution is $R^-(\bar{m})$.

To show how accurate these findings are, I have plotted the errors in Figure 27.

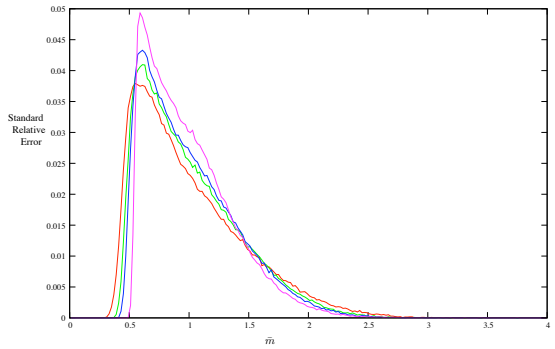

Figure 27: **Standard Error Against** $\bar{m}$
The red line is for the velocity $v_i = \frac{1}{m_i}$, green for $v_i = \frac{1}{(m_i)^2}$, blue for $v_i = \frac{1}{(m_i)^3}$ and lilac for $v_i = \frac{1}{(m_i)^{10}}$.

Furthermore, Figure 28 shows the Standard Relative Error (this is the Standard Error divided by the mass distribution at each $\bar{m}$);

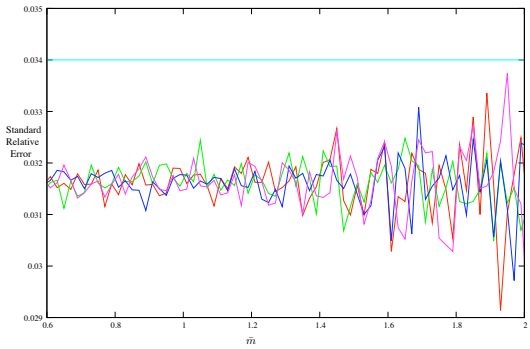

Figure 28: **Standard Relative Error Against** $\bar{m}$
The red line is for the velocity $v_i = \frac{1}{m_i}$, green for $v_i = \frac{1}{(m_i)^2}$, blue for $v_i = \frac{1}{(m_i)^3}$ and lilac for $v_i = \frac{1}{(m_i)^{10}}$. The horizontal line at 0.034 highlights that this is the maximum error.

Until this point, all the information has been gathered using the histogram method. To check for consistency, we present the results using an alternative method, the Kernel Density (KD) method, which is another way of estimating the pdf's. In this method the KD approximation of its pdf is;

$$f(x;\{x_i\},h) = \frac{1}{Nh}\sum_{i=1}^{N} K\left(\frac{x-x_i}{h}\right)$$

where K is some kernel and h is a smoothing parameter called the bandwidth. In our case $h = \frac{0.4}{(N_{total})^{\frac{1}{5}}}$ according to [16] and $N_{total} = No.ofParticles$ x $No.ofRuns$. We have taken K to be;

$$K(x) = \frac{1}{\sqrt{2\pi}}\exp\left(-\frac{x^2}{2}\right).$$

The program has been set up to calculate the standard error using the following formula;

$$SE_{kd} := \frac{1}{\sqrt{N-1}}\left[\frac{1}{h}\left(\frac{1}{N}\sum_{i=1}^{N}\frac{1}{h}K\left(\frac{x-x_i}{h}\right)^2\right) - f(x;\{x_i\},h)^2\right]^{\frac{1}{2}}$$

The error envelope for the KD method is calculated using $f(x;\{x_i\},h) - SE_{kd}$ and $f(x;\{x_i\},h) + SE_{kd}$. The consistency is demonstrated since it is clear from Figure 29 (for Velocity Exponent $p = 1$) that both methods give similar values but since the KD method provides smoother graphs and smaller errors I will use it.

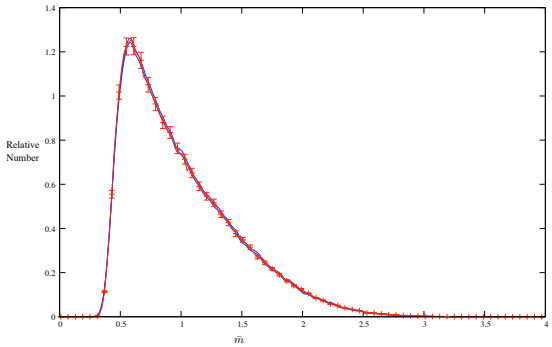

Figure 29: **Expected Mass Distribution with Standard Error and KD Error** This is for the velocity $v_i = \frac{1}{m_i}$. The red line is the histogram method distribution and red error bars are from the histogram method. The blue lines are the lower and upper KD distributions.

Figure 30 is the same for Velocity Exponent $p = 5$, just to clarify that it is accurate for all values of p;

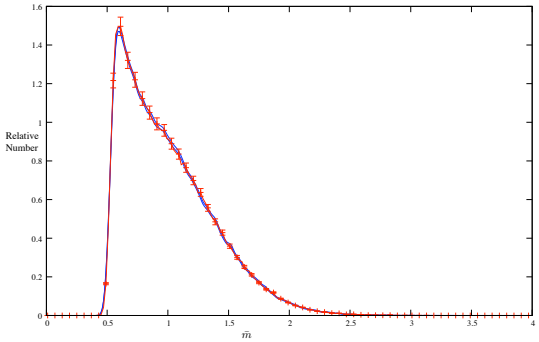

Figure 30: **Expected Mass Distribution with Standard Error and KD Error** This is for the velocity $v_i = \frac{1}{(m_i)^5}$. The red line is the histogram method distribution and red error bars are from the histogram method. The blue lines are the lower and upper KD distributions.

We have found the KD method to be superior to the Histogram method so I will use the KD method to investigate characteristic features of the scaling states.

3.11 Characteristic Features of the Scaling Functions

While examining the expected mass distributions it was noticed that there are many features that would be interesting to explore in further detail, for example, the vacuum interval and the decaying tail.

3.12 The Vacuum Interval

Here we examine the dependence of the extent of the vacuum interval on the choice of velocity law, $v_i = \frac{1}{m_i{}^p}$. From Figure 31, it can be seen that as the Velocity Exponent (p) increases, then V_p (the first point where mass is recorded) also increases and the function $f(x) = \frac{c}{(x+a)^p} + b$ is a very good fit to the graph. In this case $a = 4.1669$, $p = 2.11438$, $b = 0.494267$ and $c = -5.28102$. To get our data we have used a program to find the root which specifies that only 0.001% of the mass is to the left of this root as it is impossible to find exactly the first point where mass is recorded. From our data, $f(0.1) = 0.2486946$ and $f(28) = 0.4908277$. The above function gives $f(0.1) = 0.2485583$ and $f(28) = 0.4908355$ so it can be seen from these values that the function is a good fit.

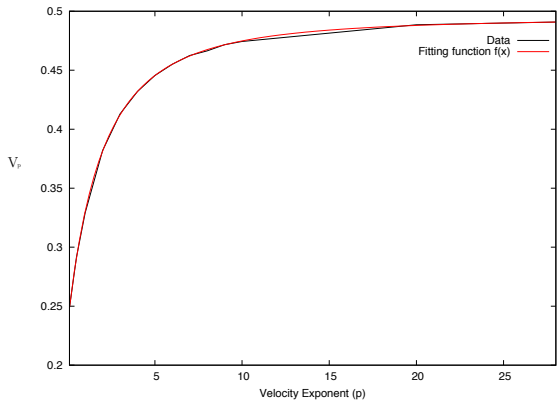

Figure 31: **Beginning of the vacuum state V_p versus the velocity exponent p** The black line is taken from our generated data and the red line is the associated least squares best fit function $f(x) = \frac{c}{(x+a)^p} + b$ where $a = 4.1669, b = 0.494267, c = -5.28102$ and $p = 2.11438$.

3.13 The Support of the Mass Distribution

While investigating the decay of the tail part of the graph, I found that if we calculate the point at which 25% of the particles remained and the point at which 5% of the particles remained, we can fit a function to this. We cannot go any lower than 5% remaining because after this point there are not enough particles left to give statistically significant data. Figure's 32 and 33 are the graphs highlighting the values at 25% remaining and the values at 5% remaining for $p = 1, .., 10$. Hence it can be seen, as expected, that as p increases the start value increases and also the value at which 25% and 5% remain decreases. After trying to fit various families of functions to the above data and consideration and analysis of the errors associated with each fitting function, I found that the

following function was reasonably accurate;

$$f(x) = f\ exp^{l_6 x^3}$$

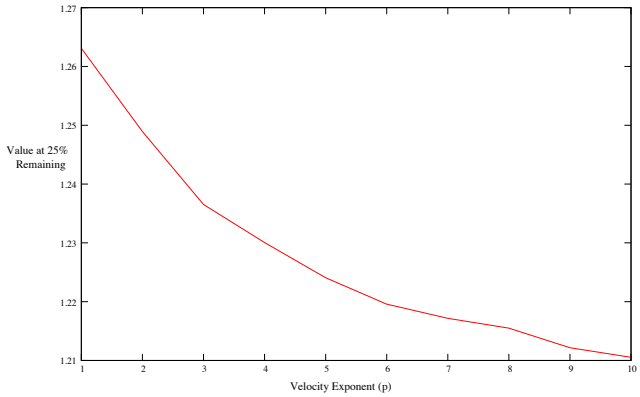

Figure 32: **Velocity Exponent (p) Against Value at 25% Remaining**
Values at 25% of the particles remaining for $p = 1, .., 10$.

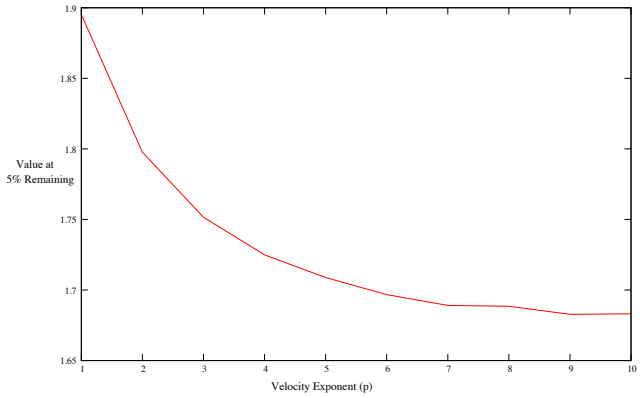

Figure 33: **Velocity Exponent (p) Against Value at 5% Remaining**
Values at 5% of the particles remaining for $p = 1, .., 10$.

4 **The $\mathcal{CRP}$ model

Here, a countable array of (massless) points on the line, x_i, is governed by a nearest neighbour dynamical system

$$\dot{x}_i = \mathscr{F}(l_i) - \mathscr{F}(l_{i-1}),$$

$$\dot{x}_i = \mathscr{F}(x_{i+1} - x_i) - \mathscr{F}(x_i - x_{i-1})$$

where l_i , l_{i-1} are the distances to the *ith* partricles right and left neighbour respectively, and where $\mathcal{F}$ is a prescribed function. Further, when particles meet they annihilate one another; denoted by the coarsening law $\oplus$

$$x_i \oplus x_{i+1} \longrightarrow \emptyset$$

Here we will focus on the unstable Allen-Cahn particle model case, first identified in [15], for which

$$\mathcal{F}(l) = \pm e^{-l}.$$

The $\mathcal{CRP}$ model is different to the $\mathcal{CBP}$ model in that the $\mathcal{CRP}$ model cannot be reduced to a canonical problem. Also the particles in the $\mathcal{CRP}$ model do not have a mass. Suppose we have an infinite number of particles on the real line. Then the set of all particles can be represented by $\{ x_i ; i \in \mathcal{I} \}$ where $\mathcal{I} \subset \mathbb{Z}$ and $\mathcal{I}$ is the index set, and x_i is the location of the i-th particle. This is shown in Figure 34.

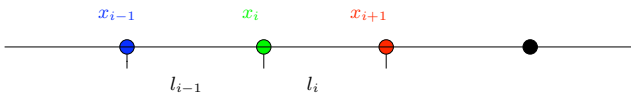

Figure 34: **Particles on a Line**
$x_{i-1} < x_i < x_{i+1}$.

We consider the domain $[0, L]$ which we simulate with L large. This is fine as long as the average particle separation $<l> << L$. Sampling the statistics requires two things; firstly that the transient associated with the initial condition is gone and this is guaranteed by making sure that $<l>_{sample} << L$ and secondly, that at the point of sampling we have separation of scale. Hence in summary we want $<l>_{initial} << <l>_{sample} << L$.

4.1 Overview

In the next section I am going to consider general information about the $\mathcal{CRP}$ model. Since it cannot be reduced to a canonical problem there are a family of problems depending on domain size to be analysed. Following on from this, I will determine if and when a scaling state occurs and I will examine the pdf's produced and how these vary depending on the domain size.

The domain in the $\mathcal{CBP}$ model was $[0, 1]$ whereas in this model the code we have enables us to vary the domain. For example, if the domain length was 10 and we wanted the average distance between particles to be 0.1, we would tell the program to output at 100 particles. In this way we can analyse the pdf at various average lengths and at various fractions as we can start the program with $200, 500, 1000, 2000, 10000$ particles and then outputting at 100 particles means that the fractions would be $\frac{1}{2}, \frac{1}{5}, \frac{1}{10}, \frac{1}{20}, \frac{1}{100}$. Figure 35 shows that coarsening is taking place as it can be seen that particles are colliding and annihilating each other.

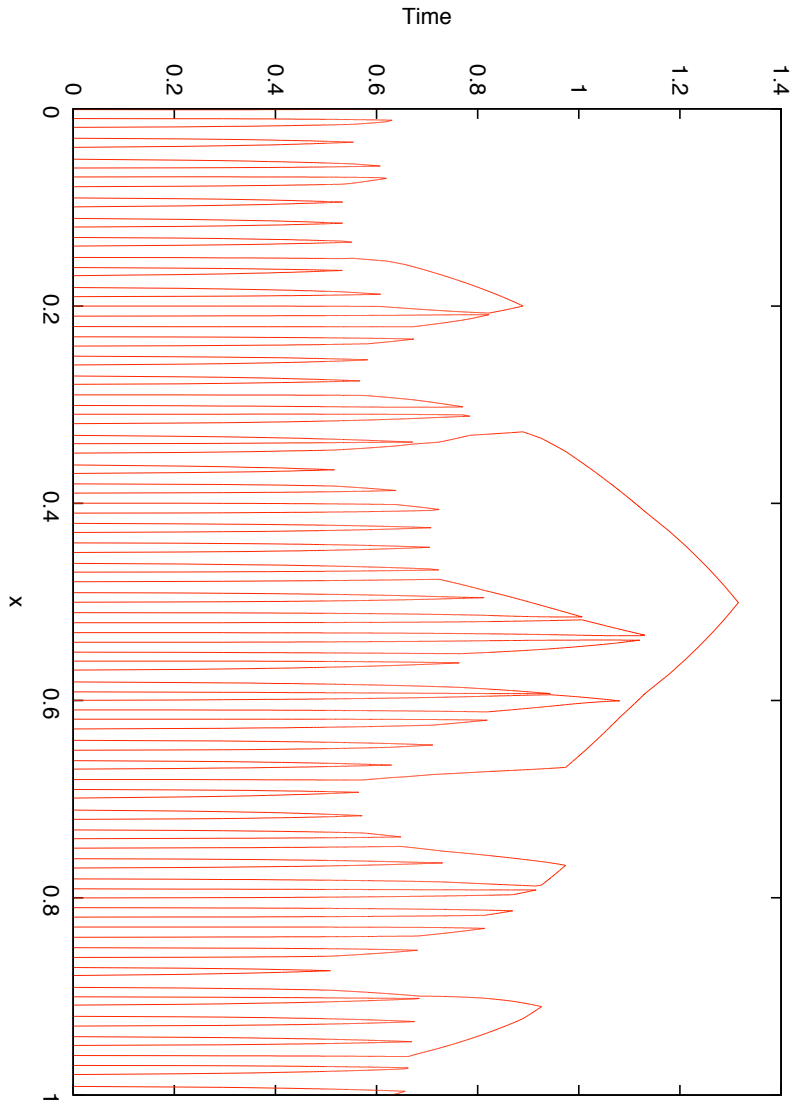

Figure 35: **Coarsening**
As can be seen from the diagram, 2 particles are colliding and annihilating each other at many different times and locations, until none remain. There were 100 particles initially.

4.2 The Particular Case of Domain Length 100

Here we are going to consider the case of domain length 100 and highlight by examining the graphs of No. of Particles against Time that there is no power law and thus no dynamic scaling. We can see from Figure 36 (which has 10000 particles at the start) how the number of particles decreases with time.

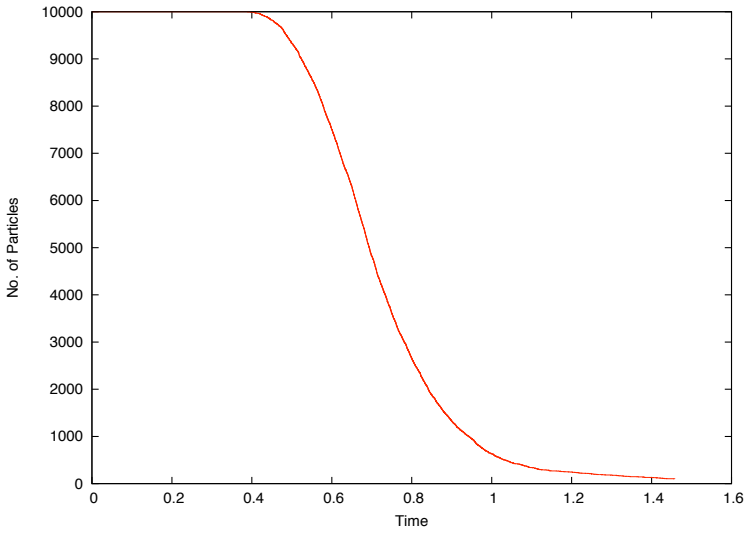

Figure 36: **Number of Particles against Time**
$N(0) = 10000$. Domain Length 100.

This is clarified by Figure 37 which has 2000 particles at the start and Figure 38 which has 1000 particles at the start.

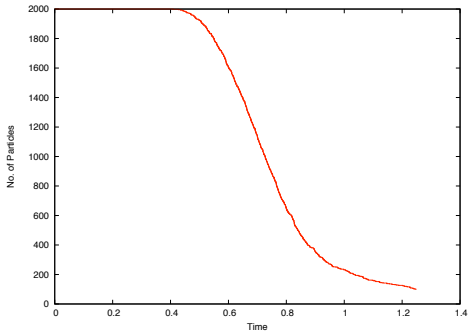

Figure 37: **Number of Particles against Time**
$N(0) = 2000$. Domain Length 100.

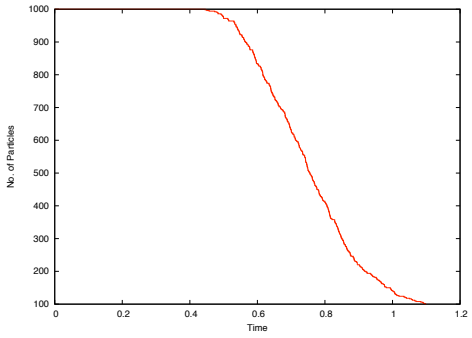

Figure 38: **Number of Particles against Time**
$N(0) = 1000$. Domain Length 100.

It is obvious from these graphs that there is not a part of this graph which straightens out (unlike the $\mathcal{CBP}$ model) and hence there is no power law. Thus this implies that there is no dynamic scaling apparent. However it can be seen from Figure 39 that if the Fraction of Particles was plotted against Time for various number of particles at the start they are all the same except from varying by a time interval.

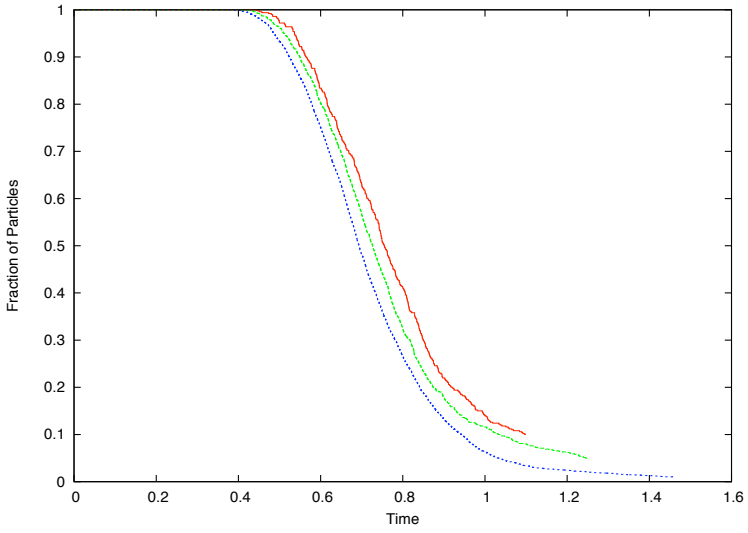

Figure 39: **Fraction of Particles against Time**
Domain Length 100. The blue line had $N(0) = 10000$, green had $N(0) = 2000$ and red had $N(0) = 1000$.

Figure 40 highlights that if we plot a cubic function along with our data then it is obvious that the cubic function f(x) is a very good fit to our data between 0.6 and 0.85. The cubic function has been fitted to 1000 particles at the start;

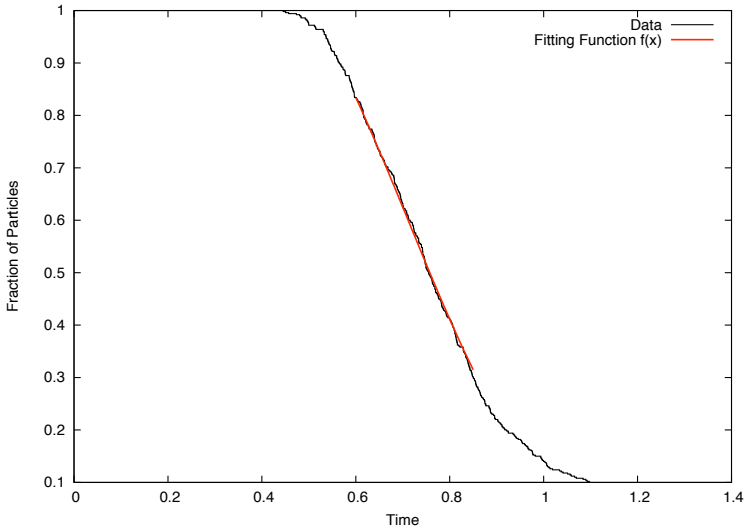

Figure 40: **Fraction of Particles against Time**
Domain Length 100. f(x) fitted to 1000 particles at the start.

4.3 Domain Length 1, 10 and 1000

Next we are going to examine the dependence on varying the domain length, L. The graph in Figure 41 highlights that as we vary the domain length, the number of particles still decreases in a similar manner as we have domain lengths of $1, 10, 100, 1000$.

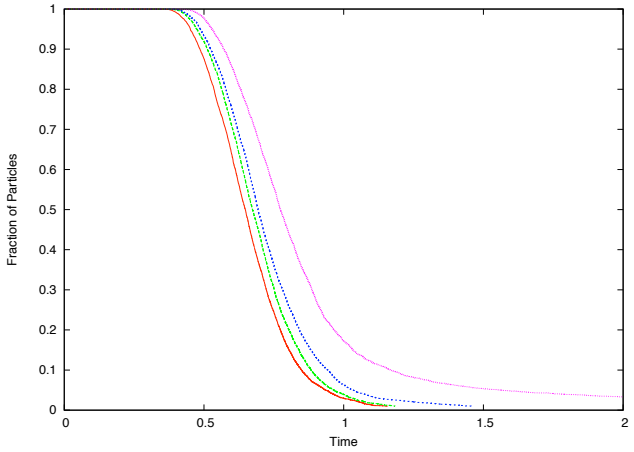

Figure 41: **Fraction of Particles against Time**
$N(0) = 10000$. The red line is Domain Length, $L = 1$. The green line is $L = 10$. The blue line is $L = 100$ and finally, the lilac line is $L = 1000$.

However it is seen from this graph that as the Domain Length increases, it takes longer for the number of particles to start decreasing. This is as expected, because as the Domain Length increases, the particles are further away from each other and hence, do not collide as quickly. Also the velocity the particles move at is decreased as the Domain Length increases, and thus again the particles are less likely to collide.

4.4 Probing the Coarsening Pathway

Furthermore, if we compare the pdf's which are all outputted at the same number of particles, but have different domain sizes and hence different average lengths between particles, then it can be seen that the distributions reflect an average length dependence (Figure 42). If we compare a number of pdf's, all

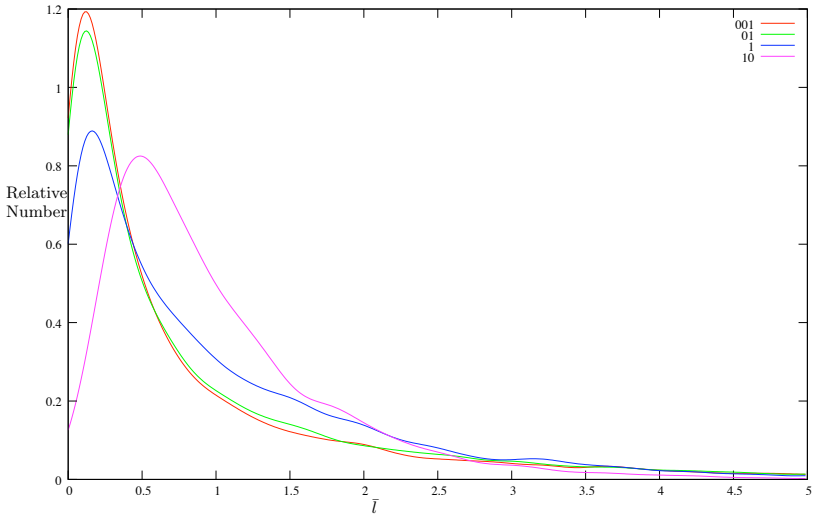

Figure 42: **Expected Length Distributions**
The key on the graph highlights that the average lengths between particles are 0.01, 0.1, 1 and 10.

outputted at 100 particles, with domain of length 1000 and thus average length 10, but all starting with a different number of particles it is obvious that the pdf varies greatly depending on the fraction of particles remaining. It seems that the pdf goes through a variety of forms before reaching a universal shape. We shall call this process the Transient and the next section shall explore this.

4.5 Exploring the Transient

Thus our first graph, in Figure 43, is outputted at 100 particles, with domain of length 1000 and thus average length 10. It is collated when $\frac{1}{2}$ of the particles are remaining ie there were 200 particles to start with.

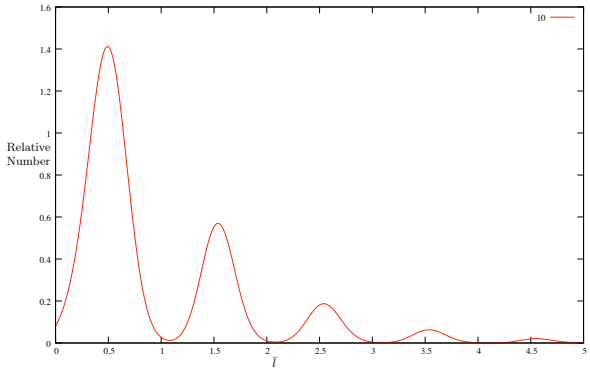

Figure 43: **Expected Length Distribution**
Outputted at 100 particles but with 200 particles at the start. Domain Length, $L = 1000$. Average Length, 10.

The next graph, in Figure 44, is outputted at 100 particles, with domain of length 1000 and thus average length 10. Figure 44 shows the pdf when $\frac{1}{5}$ of the particles are remaining so there were 500 particles at the start.

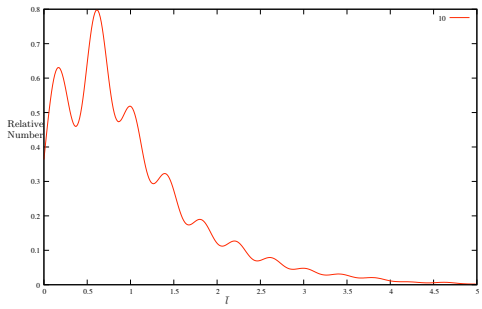

Figure 44: **Expected Length Distribution**
Outputted at 100 particles but with 500 particles at the start. Domain Length, $L = 1000$. Average Length, 10.

In Figure 45 it can be seen that a more universal shape is being reached. This graph is plotted when 100 particles remain, the domain is of length 1000 and the average length 10. Hence Figure 45 shows the pdf when $\frac{1}{100}$ of the particles are remaining, so there were 10000 at the start.

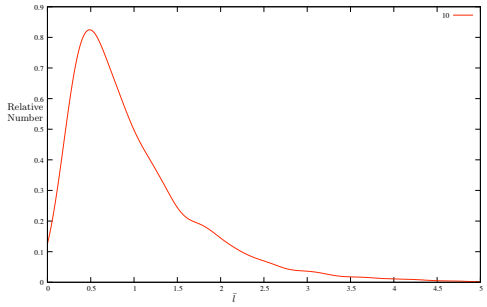

Figure 45: **Expected Length Distribution**
Outputted at 100 particles but with 10000 particles at the start. Domain Length, $L = 1000$. Average Length, 10.

However, because the domain length and average length in these cases is very large it takes a long time for the profile to get to the universal shape.

Another case which moves much quicker is the domain length 1 and average length 0.01, obviously outputted at 100 particles. Thus Figure 46 shows the pdf when $\frac{1}{100}$ of the particles are remaining, ie there were 10000 particles at the start.

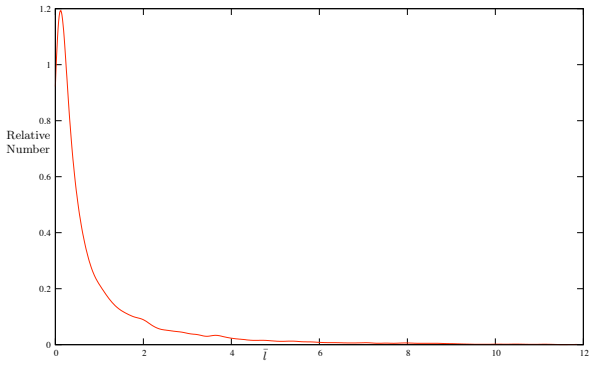

Figure 46: **Expected Length Distribution**
Outputted at 100 particles but with 10000 particles at the start. Domain Length, $L = 1$. Average Length, 0.01.

If we fit a function to the tail of the graph in Figure 46, between 2.5 and 12, we find that $f(x) = \frac{a}{x^p}$ is a good fit and in the case shown in Figure 47, $a = 0.409684$ and $p = 2.11599$. It is interesting just to note that the tail actually goes out to about 33 times the average.

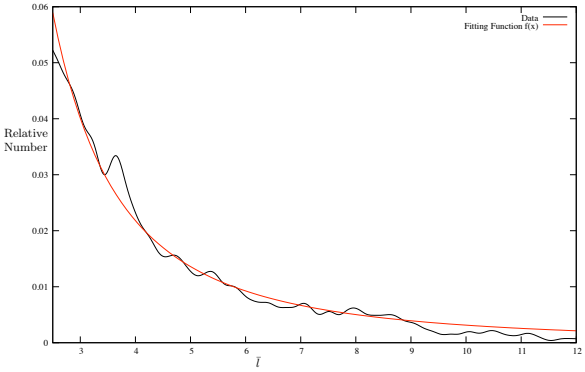

Figure 47: **Fitting to Expected Length Distribution**
Outputted at 100 particles but with 10000 particles at the start. Domain Length, $L = 1$. Average Length, 0.01. Our data is in red and the fitting function $f(x) = \frac{a}{x^p}$ is in black.

References

[1] K. Pesz & G. J. Rodgers, J. Phys. A: Math. Gen. **25**, 705-713 (1992).

[2] B. Derrida & C. Godreche & I. Yekutieli, Phys. Rev. A. **44**, 6241-6251 (1991).

[3] B. Derrida & C. Godreche & I. Yekutieli, Europhys. Lett. **12**, 385-390 (1990).

[4] I. Yekutieli & C. Godreche & B. Derrida, Phys. A. **185**, 240-244 (1992).

[5] www.process-evolution.com/plentehome.html

[6] www.grc.nasa.gov/WWW/RT/RT2002/6000/6728hickman.html

[7] G. L. Thomas & R. M. C. de Almeida, Phys. Rev. E. **74**, 021407 (2006).

[8] A. Cervantes Martinez & E. Rio & G. Delon & A. Saint-Jalmes & D. Langevin & B. P. Binks, Soft Matter **4**, 1531-1535 (2008).

[9] J. Lambert & R. Mokso & I. Cantat & P. Cloetens & J. A. Glazier & F. Graner & R. Delannay, Coarsening foams robustly reach a self-similar growth regime. Preprint (2009).

[10] A. Saint-Jalmes, Soft Matter **2**, 836-849 (2006).

[11] D. J. Durian & D. A. Weitz & D. J. Pine, Phys. Rev. A. **44**, 7902-7905 (1991).

[12] Robert K. Prud'homme & Saad A. Khan, Foams : Theory, Measurements, and Applications. Surfactant Science Series **57**, (1996).

[13] A. J. Bray, Adv. Phys. **43**, 357 (1994).

[14] S. J. Watson & F. Otto & B. Y. Rubinstein & S. H. Davis, Physica D. **178**, 127-148 (2003).

[15] K. Kawasaki & T. Nagai, Physica. **121A**, 175-206 (1983).

[16] http://en.wikipedia.org/wiki/Kernel$_d ensity$